Role of Nonlinear Coupling and Density Fluctuations in Magnetic-Fluctuation-Induced Particle Transport

L. Lin, W. X. Ding, D. L. Brower, W. F. Bergerson, T. A. Carter, T. F. Yates, A. F. Almagri, B. E. Chapman, and J. S. Sarff

Phys. Rev. Lett. **108**, 175001 — Published 23 April 2012

DOI: 10.1103/PhysRevLett.108.175001

Role of Nonlinear Coupling and Density Fluctuations in Magnetic-Fluctuation-Induced Particle Transport

L. Lin, W. X. Ding, D. L. Brower, W. F. Bergerson,
T. A. Carter, T. F. Yates
Department of Physics and Astronomy, University of California Los Angeles,
Los Angeles, California 90095

A. F. Almagri, B. E. Chapman, J. S. Sarff
Department of Physics, University of Wisconsin-Madison,
Madison, Wisconsin 53706

Abstract

Three-wave nonlinear coupling among spatial Fourier modes of density and magnetic fluctuations is directly measured in a magnetically-confined toroidal plasma. Density fluctuations are observed to gain (lose) energy from (to) either equilibrium or fluctuating fields depending on mode number. Experiments indicate that nonlinear interactions alter the phase relation between density and magnetic fluctuations, leading to strong particle transport.

Magnetic-fluctuation-induced particle transport is an increasingly important topic in astrophysics [1] and high-temperature laboratory plasma research [2]. For magnetically-confined fusion plasmas, magnetic fluctuations arising from microtearing modes [3], global tearing modes [4], energetic-particle-induced instabilities [5], as well as from external-coil-induced resonant-magnetic perturbations used to mitigate edge-localized modes [6], can all act to enhance particle transport. In addition, magnetic fluctuations leading to a stochastic magnetic field have also been observed in recent gyrokinetic simulations of drift-wave type of turbulence, after inclusion of finite pressure effects [7]. The effect of magnetic fluctuations on particle transport is predicted to increase with β (ratio of plasma pressure to magnetic field pressure) and for burning plasmas where 3.5 MeV α-particles are available to drive instabilities [8]. Understanding the physics of particle transport associated with magnetic fluctuations is critical for maintaining plasma confinement, density control and impurity exhaust in burning plasmas like ITER and beyond.

Direct measurements of magnetic-fluctuation-induced transport in high-temperature plasmas are rare [4], being largely limited by methods available to access the hot plasma core. Recent measurements [9] have established that magnetic-fluctuation-induced particle transport, arising from the correlated product of density and magnetic fluctuations, is the cause of the density profile relaxation during sawtooth crashes in the reversed-field pinch (RFP). In spite of different magnetic topologies, sawtooth crashes on RFPs and tokamaks have many common features, including density and current profile relaxation as well as increased turbulence [10, 11]. During the crash, the RFP magnetic field is strongly stochastic and the phase between density and magnetic fluctuations is observed to change so as to induce transport. In addition, the observed particle transport [9] is much larger than expected from the quasi-linear prediction [12] for ambipolar particle transport in a stochastic field, suggesting that coherent, nonlinear, mode-mode interactions might serve to drive this transport.

Nonlinear interactions between density and electrostatic potential fluctuations associated with drift-wave turbulence have been extensively studied previously ([13, 14] and references therein). In this Letter, we report on direct measurements of a broad spectrum of nonlinear three-wave interactions between density and magnetic fluctuations

associated with global tearing instabilities. Energy exchange between different spatial Fourier modes resulting from nonlinear interactions acts to drive or damp density fluctuations, depending on mode number. These measurements reveal that the effects of nonlinear three-wave interactions are comparable to linear advection where energy exchange with the equilibrium density gradient occurs. Nonlinear interactions are observed to alter the phase relation between density and magnetic fluctuations so as to drive large particle transport.

Following a similar approach as in [15] and starting from the continuity equation for incompressible electrons ($\nabla \cdot \mathbf{\upsilon}_e \simeq 0$), we can write

$$\frac{\partial n_e}{\partial t} + \mathbf{\upsilon}_e \cdot \nabla n_e \simeq S_e , \tag{1}$$

where n_e, $\mathbf{\upsilon}_e$, and S_e are the electron density, velocity and source term, respectively. n_e and $\mathbf{\upsilon}_e$ can be decomposed into their equilibrium (n_0 and $\mathbf{\upsilon}_0$) and fluctuating ($\tilde{n}_k$ and $\tilde{\mathbf{\upsilon}}_k$) components, i.e. $n_e = n_0 + \Sigma_k \tilde{n}_k$ and $\mathbf{\upsilon}_e = \mathbf{\upsilon}_0 + \Sigma_k \tilde{\mathbf{\upsilon}}_k$, where $k = (m,n)$, and m, n are the poloidal and toroidal mode numbers, respectively. Here, we focus on the radial velocity fluctuations ($\tilde{\upsilon}_r$) associated with particles streaming along the magnetic field. From the field line equation we obtain $\tilde{\upsilon}_r = \upsilon_{e\|} \tilde{b}_r / B_0$, where $\upsilon_{e\|}$ denotes the parallel electron drift velocity along the field line, $\tilde{b}_r$ is the radial magnetic fluctuation, and B_0 is the equilibrium magnetic field. After substituting the decomposed n_e and $\mathbf{\upsilon}_e$ into Eq. (1), multiplying by $\tilde{n}_{k_1}$, substituting for $\tilde{\upsilon}_r$, and performing an average $\langle \ldots \rangle$ over the magnetic flux surface, we have the energy equation for electron density fluctuations,

$$\frac{1}{2}\frac{\partial \left\langle \tilde{n}_{k_1}^2 \right\rangle}{\partial t} \simeq -\frac{\upsilon_{e\|}}{B_0}\left\langle \tilde{n}_{k_1} \tilde{b}_{r,k_1} \right\rangle \frac{\partial n_0}{\partial r} - \frac{\upsilon_{e\|}}{B_0} \sum_{k_1 = k_2 \pm k_3} \left\langle \tilde{n}_{k_1} \tilde{b}_{r,k_2} \frac{\partial \tilde{n}_{k_3}}{\partial r} \right\rangle . \tag{2}$$

Contributions from the source, higher-order nonlinear interactions (such as four-wave coupling), and dissipation effects are not considered in Eq. (2). The left-hand side of Eq. (2) is the power term describing the temporal evolution of modal energy residing in $\tilde{n}_{k_1}$.

The first term on the right-hand side is the linear advection, which accounts for the energy exchange between $\tilde{n}_{k_1}$ and the equilibrium density gradient $\partial n_0 / \partial r$. This term can also be written as $-\Gamma_{k_1} \partial n_0 / \partial r$, where $\Gamma_{k_1} = \upsilon_{e\|} \left\langle \tilde{n}_{k_1} \tilde{b}_{r,k_1} \right\rangle / B_0$ is the particle flux resulting from fluctuations with k_1. The second term on the right-hand side is the nonlinear advection. It is a triple product of three fluctuating quantities ($\tilde{n}_{k_1}$, $\tilde{b}_{r,k_2}$, $\partial \tilde{n}_{k_3} / \partial r$) and describes the nonlinear three-wave interaction among fluctuations with mode numbers k_1, k_2 and k_3. Depending on sign, the linear and nonlinear advection terms can act to drive or damp density fluctuations. In the following, we report on direct measurements of each term in Eq. (2).

Our experiments have been conducted in the Madison Symmetric Torus (MST) [16], a toroidal device with major radius $R = 1.5$ m and minor radius $a = 0.52$ m. All data presented herein are for deuterium RFP plasmas with toroidal plasma current 400 kA and central line-averaged electron density 1×10^{19} m^{-3}. Multiple magnetic tearing modes resonate in these plasmas. Modes with $m = 1$ and $n = 5 - 12$ resonate inside the reversal surface where the toroidal field changes direction, while modes with $m = 0$, $n = 1 - 4$ resonate at the reversal surface near $r / a \sim 0.8$, where the electron temperature is ~150 eV. The plasma exhibits a quasi-periodic "sawtooth" relaxation cycle evident in many quantities [17]. The cycle consists of a slow ramp (~4 ms) followed by a rapid relaxation or crash (~100 μs) during which the tearing modes spike to their maximum amplitudes. The multiple magnetic islands associated with these modes overlap, leading to a stochastic magnetic field [18] accompanied by strong density relaxation and particle pump-out [9].

Although tearing modes have localized resonant surfaces, their associated density ($\tilde{n}_k$) and radial magnetic fluctuations ($\tilde{b}_{r,k}$) have a global extent. All $\tilde{n}_k$ peak near the reversal surface where the equilibrium density gradient ($\partial n_0 / \partial r$) is large [19], while $\tilde{b}_{r,k}$ peaks near the corresponding resonant surface [20]. Measurements shown herein were obtained near the reversal surface where $m = 0$ modes are maximum. To illustrate typical behavior, the root-mean-square (RMS) values of $\tilde{n}$, $\tilde{b}_r$, their relative phase $\delta_{\tilde{n}\tilde{b}_r}$, and the

magnetic fluctuation-induced particle flux $\Gamma_k = \upsilon_{e\|} \left\langle \tilde{n}_k \tilde{b}_{r,k} \right\rangle / B_0$, for the $(m,n) = (1,10)$ mode, are shown in Fig. 1. The measurements are accomplished using a high-speed, laser-based, polarimetry-interferometry diagnostic. The line-integrated measurements from the outermost chord are localized to the edge region ($0.8 \le r/a \le 1$). Standard interferometry is employed to measure the equilibrium density profile and density fluctuations. Electron drift velocity along the field line ($\upsilon_{e\|}$) is determined from $\upsilon_{e\|} = J_\| / (en_0)$, where $J_\|$ is the parallel plasma current density, and e is the electron charge. Radial magnetic fluctuations $\tilde{b}_r$, equilibrium magnetic strength B_0, and $J_\|$ are each determined by measuring the Faraday effect [20, 21]. Detailed descriptions of the measurement and analysis techniques have been previously published [9, 22]. For $t \le -0.2$ ms well before the sawtooth crash at $t = 0$ ms, although $\tilde{n}$ [Fig. 1(a)] and $\tilde{b}_r$ [Fig. 1(b)] have finite amplitude, their relative phase $\delta_{\tilde{n}\tilde{b}_r}$ [Fig. 1(c)] is close to $\pi/2$, resulting in a low particle flux [Fig. 1(d)]. However, at $t = -0.06$ ms, just before the crash, $\delta_{\tilde{n}\tilde{b}_r}$ deviates from $\pi/2$ as $\tilde{n}$ and $\tilde{b}_r$ amplitudes increase, leading to maximum particle flux at the crash. Similar observations have been made for the other dominant modes ($m = 1, n = 5-12$). This burst in flux causes density profile relaxation and particle pump-out [9].

Addressing the intriguing question of why the fluctuation amplitudes and phase spontaneously change at the crash, requires investigation of driving and damping mechanisms of the density fluctuations through measurement of all terms in Eq. (2). To evaluate the linear and nonlinear terms, in addition to the results from Fig. 1, measurements of $\partial n_0 / \partial r$ and $\partial \tilde{n}_k / \partial r$ are required. $\partial n_0 / \partial r$ is obtained by inverting the line-integrated density profile, while $\partial \tilde{n}_k / \partial r$ is directly measured by using a novel differential interferometry technique [22]. The amplitude of $\partial \tilde{n}_k / \partial r$ tracks that of $\tilde{n}_k$ and peaks at the crash. After obtaining $\tilde{n}_{k_1}$, $\tilde{b}_{r,k_2}$, and $\partial \tilde{n}_{k_3} / \partial r$, their triple product can be quantitatively determined. The sign and amplitude determine the direction and strength of energy flow among the modes involved in the nonlinear interaction and is critical to understanding the underlying mechanisms of the three-wave process.

Evaluation of Eq. (2) for the $(m,n)=(1,10)$ mode reveals that each of the three terms grows significantly at the sawtooth crash, as shown in Fig. 2. Interestingly, the measured power term is much smaller than the linear and nonlinear advection terms, remaining below $0.2\times10^{40}\,\mathrm{m^{-6}s^{-1}}$. The magnitude of the linear and nonlinear terms begins to change at $t=-0.06$ ms before the crash, when $\tilde{n}$ and $\tilde{b}_r$ amplitudes increase, and their relative phase begins to deviate from $\pi/2$ [see Fig.1(a-c)]. The linear term is large and positive ($1.5\times10^{40}\,\mathrm{m^{-6}s^{-1}}$ at $t=-0.02$ ms), which indicates that the (1,10) mode is linearly unstable as it gains its energy from the equilibrium density gradient $\partial n_0/\partial r$. In contrast, the nonlinear term is negative with comparable amplitude, indicating the nonlinear interaction is a sink of energy which is transferred away from (1,10) mode to other modes through three-wave interactions. Within experimental uncertainty, the sum of the nonlinear and linear advection terms equates with the power term, thereby balancing Eq. (2).

Similar analysis of Eq. (2) has been performed for all the dominant modes as shown in Fig. 3. Here we observe the mode spectra of linear and nonlinear terms averaged over the time interval -0.04 to -0.02 ms before the sawtooth crash. The power term is always small, remaining less than 15% of either the linear or nonlinear terms. The cause of the density fluctuations varies with mode number as the linear and nonlinear advection terms can be either driving (positive) or damping (negative). Interestingly, the $m=0$, $n=1,2,3,4$ reversal-surface-resonant modes are all linearly stable and nonlinearly driven. The $m=1$ core-resonant modes exhibit less uniform behavior. Modes ($m=1$, $n=5-10$) with the longer wavelength and resonant surfaces closer to the magnetic axis are linearly unstable with nonlinear damping. Conversely, modes ($m=1$, $n=11-12$) with the shorter wavelength and resonance closer to the reversal surface are nonlinearly driven with linear damping. In all cases, the linear and nonlinear terms are of opposite sign and roughly balance, within measurement error. The energy balance of $(0,2)$ and $(0,3)$ is less resolved as the amplitude of nonlinear term is about half of that of linear term. This might be caused by possible three-wave interaction from $m\geq2$ modes

excluded in our analysis or other effects neglected in Eq. (2). Balancing linear and nonlinear advection leads to the relation

$$\Gamma_{k_1} \simeq -\frac{J_{||}}{en_0 B_0}\left(\frac{\partial n_0}{\partial r}\right)^{-1} \sum_{k_1=k_2\pm k_3} \left\langle \tilde{n}_{k_1} \tilde{b}_{r,k_2} \frac{\partial \tilde{n}_{k_3}}{\partial r} \right\rangle, \quad (3)$$

revealing the magnetic-fluctuation-induced particle flux is affected by nonlinear interactions.

Many mode combinations can satisfy the sum rule ($k_1 = k_2 \pm k_3$) for the three-wave interactions and the nonlinear terms shown in Figs. 2-3 are summed over all combinations. For example, the nonlinear interaction spectrum for the $(m,n) = (1,10)$ mode is shown in Fig. 4, at $t = -0.02$ ms, when the nonlinear interaction is strongest. The nonlinear term is negative and the energy is transferred away from the $(1,10)$ mode. The three-wave interactions with $(1,9)$ and $(1,11)$ modes have the largest amplitudes, indicating the interaction is dominated by coupling with nearby or adjacent modes through the $(0,1)$ mode. Smaller contributions come from the $(0,2)$ and $(0,3)$ modes. Similar observations have been made for modes $m = 1, n = 5-12$. To further explore the role played by the $(0,1)$ mode, we have compared sawtooth cycles where the $(0,1)$ mode peaks at the crash with those where the $(0,1)$ mode exhibits no burst, as shown in Fig. 5(a). Both crash types occur spontaneously, although those with large $(0,1)$ bursts are more typical. For these events, the core-resonant $m = 1$ modes also behave differently, as seen in Figs. 5(b) and 5(c), for the $(1,7)$ mode. Measurements demonstrate that the magnetic fluctuation increase is less pronounced and no significant particle flux is induced for the sawtooth crash where the $(0,1)$ mode burst is not evident. Furthermore, comparison of the equilibrium density evolution [see Fig. 5(d)] reveals that density relaxation (decrease of the central density at $r \sim 0$ and increase of the edge density at $r/a \sim 0.8$) is no longer observed when the $(0,1)$ mode amplitude is unchanged at the crash. For sawtooth crashes where the $(0,1)$ mode is not evident, there is no burst in particle flux and no change in equilibrium density. Combining this observation with the nonlinear spectra in Fig. 4, confirms the importance of the $(0,1)$ mode in mediating nonlinear three-wave interactions.

The nonlinear interaction is important in two aspects. First, it is responsible for phase deviation from $\pi/2$ and increased particle transport confirming Eq. (3). If only linear advection exists, the phase between density and radial magnetic fluctuations remains near $\pi/2$ and weak particle transport is induced. Second, the nonlinear interaction provides the balance for the linear advection in Eq. (2).

While the measurements presented herein were made in the environment of a stochastic magnetic field created by nonlinearly interacting tearing modes, Eq.(2) applies whether or not the field is stochastic. The particle transport described in this Letter is intrinsically associated with the coherent interaction of magnetic and density perturbations, implying that magnetic-fluctuation-induced particle transport could arise even in the absence of magnetic stochasticity. This may explain why electron transport during the sawtooth crash can exceed the ambipolar-constrained value expected for parallel streaming in a stochastic magnetic field [9].

In conclusion, direct experimental measurements of linear advection and nonlinear three-wave interactions have been made, revealing their effect on density fluctuations and magnetic fluctuation-induced particle transport. Strong nonlinear coupling among global magnetic perturbations are approximately balanced by linear advection during reconnection and lead to enhanced particle transport.

The authors wish to thank the MST group for their support and contributions to this research. This work is supported by U.S. Department of Energy.

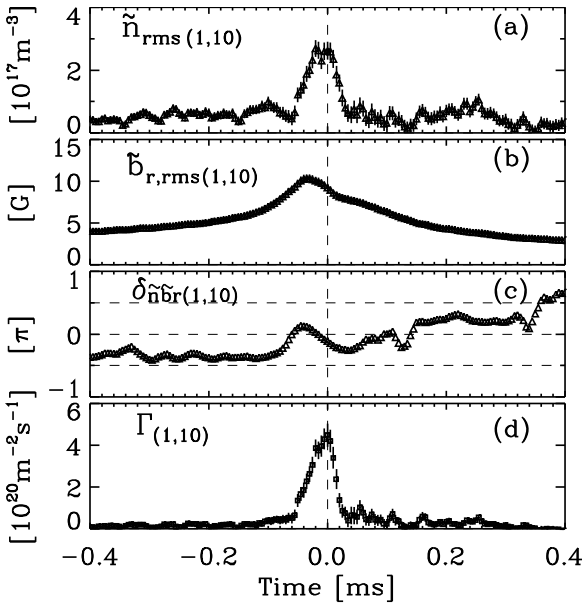

FIG.1. Temporal evolution of (a) rms value of density fluctuation ($\tilde{n}$); (b) rms value of radial magnetic fluctuation ($\tilde{b}_r$); (c) phase between $\tilde{n}$ and $\tilde{b}_r$; (d) magnetic-fluctuation induced particle flux from the $(m,n)=(1,10)$ mode at $r/a \sim 0.8$ during the sawtooth cycle. Crash occurs at $t=0$.

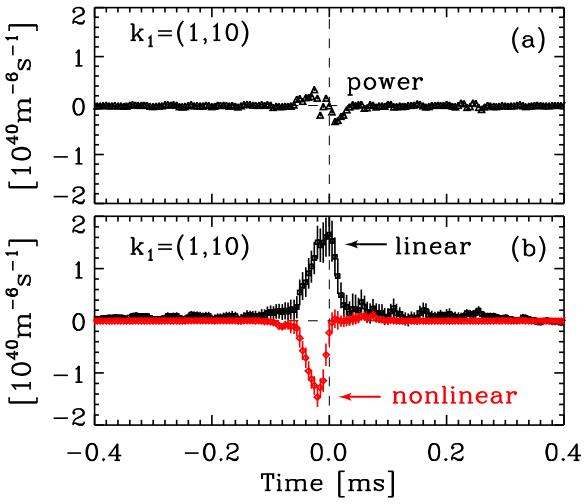

FIG. 2 (color online). Temporal evolution of (a) power term, (b) linear (black) and nonlinear (red) advection terms for the $(m,n)=(1,10)$ mode at $r/a\sim 0.8$ during a sawtooth cycle. Crash occurs at $t=0$.

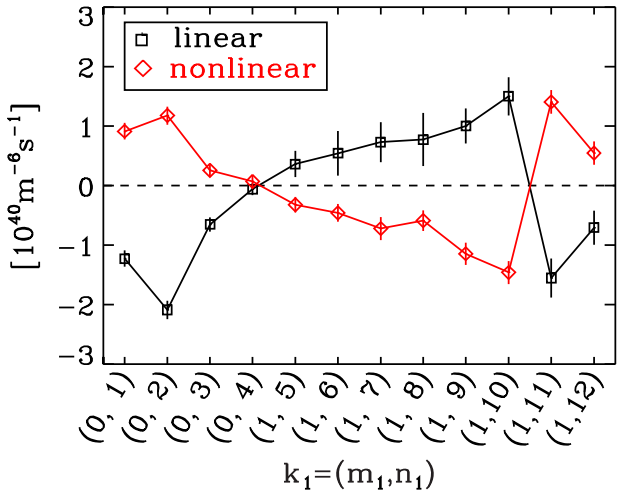

FIG. 3 (color online). Spectra of linear and nonlinear terms before the crash. Data are averaged over interval $t = -0.04$ ms to $t = -0.02$ ms before the sawtooth crash.

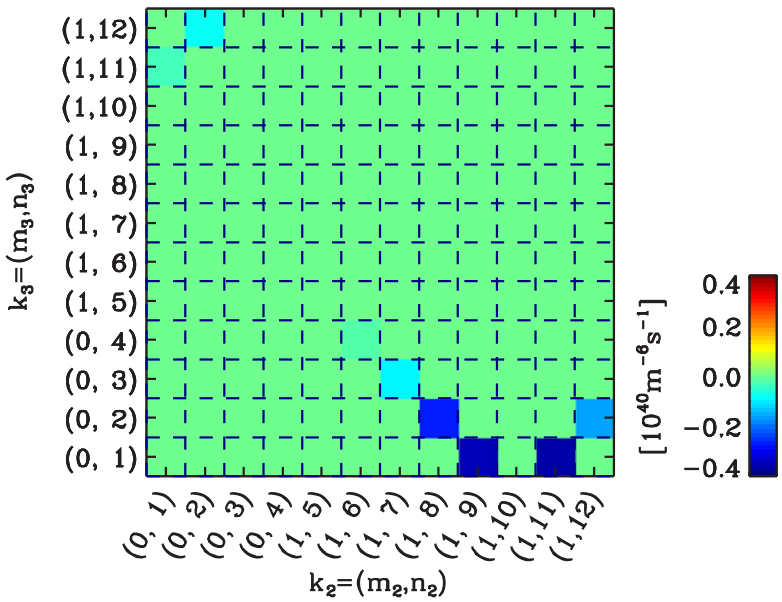

FIG. 4 (color online). Mode spectrum of nonlinear interaction for the $k_1 = (1,10)$ mode at $t = -0.02$ ms and $r/a \sim 0.8$.

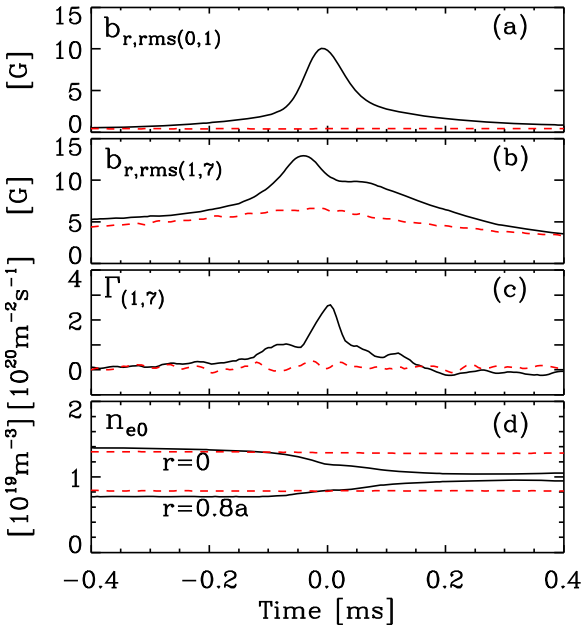

FIG. 5 (color online). Temporal evolution of (a) (0,1) radial magnetic fluctuation; (b) (1,7) radial magnetic fluctuation; and (c) (1,7) mode magnetic-fluctuation induced particle flux at $r/a \sim 0.8$. (d) Equilibrium electron density at the core ($r \sim 0$) and reversal surface ($r/a \sim 0.8$) for two types of sawtooth cycles: with strong (0,1) burst (black solid line) and without (0,1) burst (red dashed line) at $t = 0$.

[1] E. P. Kontar, I. G. Hannah, and N. H. Bian, Astrophys. J. Lett. **730**, L22 (2011).
[2] B. A. Carreras, IEEE Trans. Plasma Sci. **25**, 1281 (1997).
[3] W. Guttenfelder *et al.*, Phys. Rev. Lett. **106**, 155004 (2011).
[4] M. R. Stoneking *et al.*, Phys. Rev. Lett. **73**, 549 (1994).
[5] W. Heidbrink, Phys. Plasmas **15**, 055501 (2008).
[6] T. E. Evans *et al*., Phys. Rev. Lett. **92**, 235003 (2004).
[7] W. M. Nevins, E. Wang, and J. Candy, Phys. Rev. Lett. **106**, 065003 (2011).
[8] W. W. Heidbrink and G. J. Sadler, Nucl. Fusion **34**, 535 (1994).
[9] W. X. Ding *et al.*, Phys. Rev. Lett. **103**, 025001 (2009).
[10] D. L. Brower *et al.*, *et al*., Phys. Rev. Lett. **65**, 337 (1990).
[11] B. W. Rice, E. B. Hooper, Nucl. Fusion **34**, 1 (1994).
[12] R. W. Harvey, M. G. McCoy, J. Y. Hsu, and A. A. Mirin, Phys. Rev. Lett. **47**, 102 (1981).
[13] G. R. Tynan, A. Fujisawa and G. McKee, Plasma Phys. Control. Fusion **51**, 113001 (2009).
[14] A. Fujisawa Plasma Phys. Control. Fusion **53**, 124015 (2011).
[15] C. Holland *et al.*, Phys. Plasmas **14**, 056112 (2007).
[16] R. N. Dexter *et al.*, Fusion Technol. **19**, 131 (1991).
[17] S. Choi, D. Craig, F. Ebrahimi, and S. C. Prager, Phys. Rev. Lett. **96**, 145004 (2006).
[18] T. M. Biewer *et al.*, Phys. Rev. Lett. **91**, 045004 (2003).
[19] N. E. Lanier *et al.*, Phys. Plasmas **8**, 3402 (2001).
[20] W. X. Ding *et al.*, Phys. Rev. Lett. **93**, 045002 (2004).
[21] D. L. Brower *et al.*, Phys. Rev. Lett. **88**, 185005 (2002).
[22] L. Lin *et al.*, Rev. Sci. Instrum. **81**, 10D509 (2010).